

Unlocking photoanode performance through a roadmap for electrophoretic deposition of carbon nitride/tungsten oxide heterojunction thin films

Madasamy Thangamuthu*, Tara M LeMercier, Emerson C Kohlrausch, Samuel Lewis, Matthew Macfarlane, Andrei N Khlobystov*

School of Chemistry, University of Nottingham, University Park, Nottingham NG7 2RD, United Kingdom

Supporting information

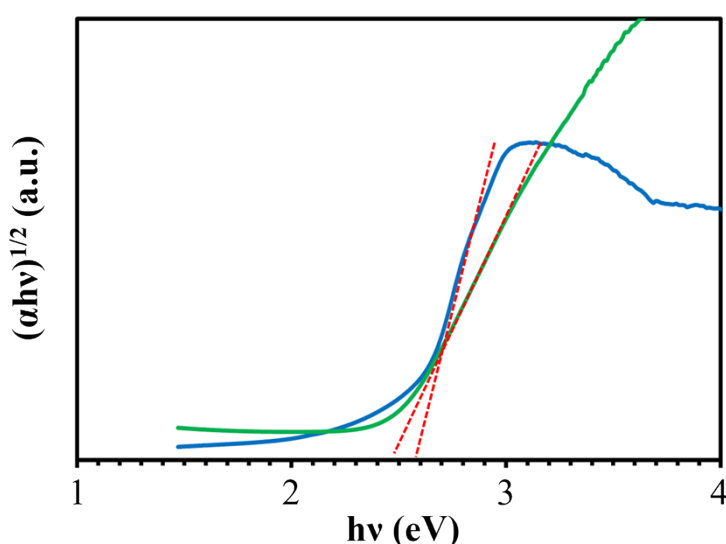


Fig. S1 Tauc plots of the $g\text{-C}_3\text{N}_4$ (blue) and WO_3 (green).

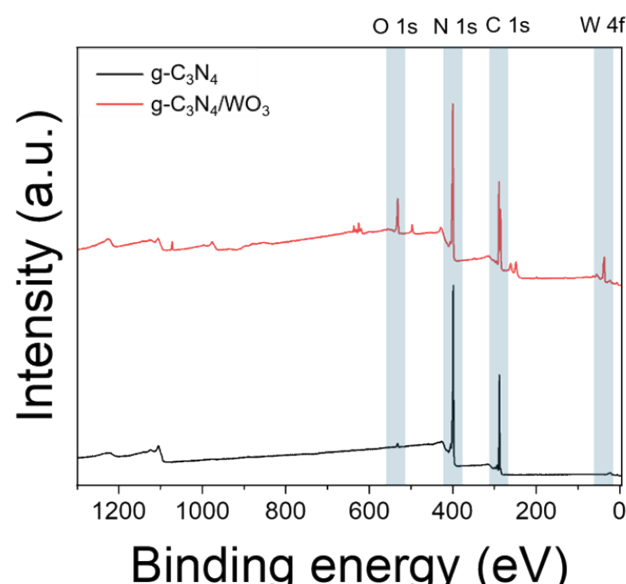


Fig. S2 XPS survey spectra of $g\text{-C}_3\text{N}_4$ and $g\text{-C}_3\text{N}_4/\text{WO}_3$

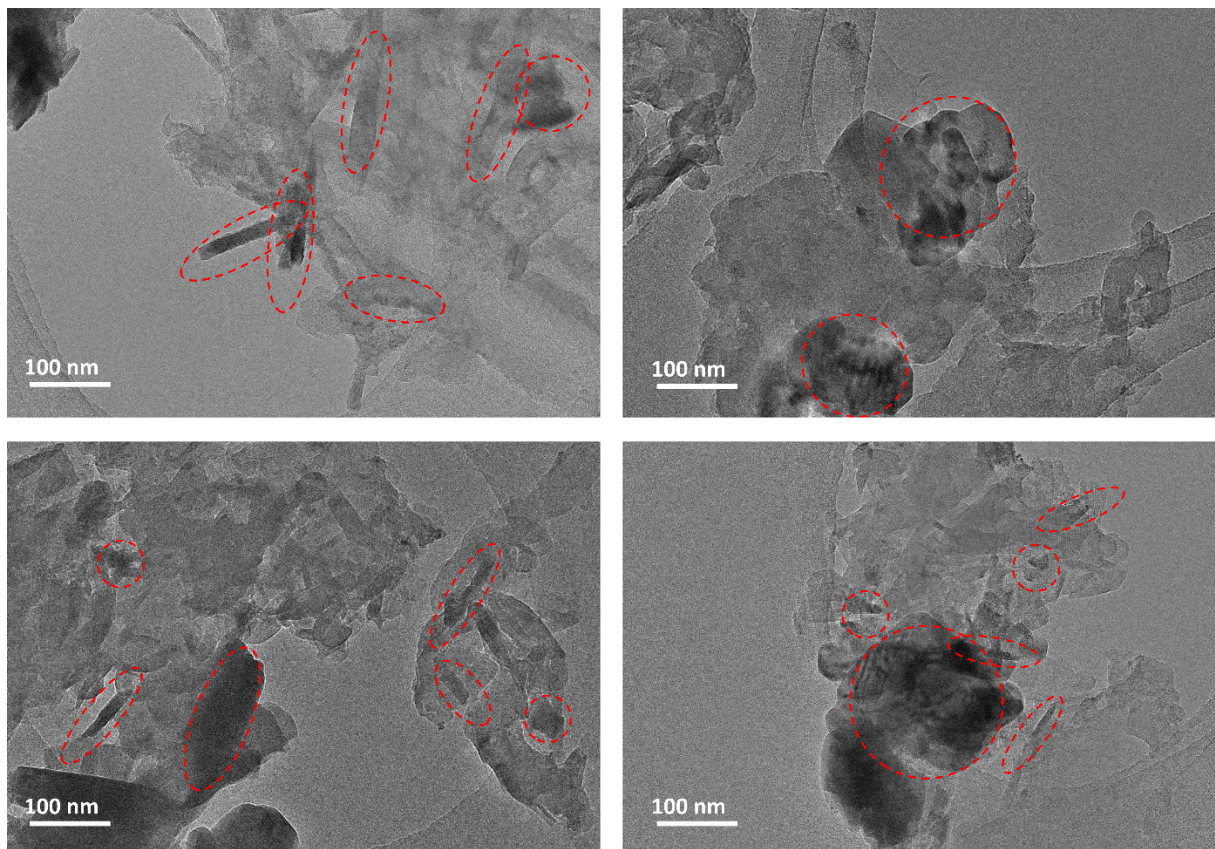


Fig. S3 TEM images of $\text{g-C}_3\text{N}_4/\text{WO}_3$. Areas of low contrast correspond to $\text{g-C}_3\text{N}_4$. Whilst areas of high contrast correspond to WO_3 , some of which are highlighted (red dashed shapes) for clarity.

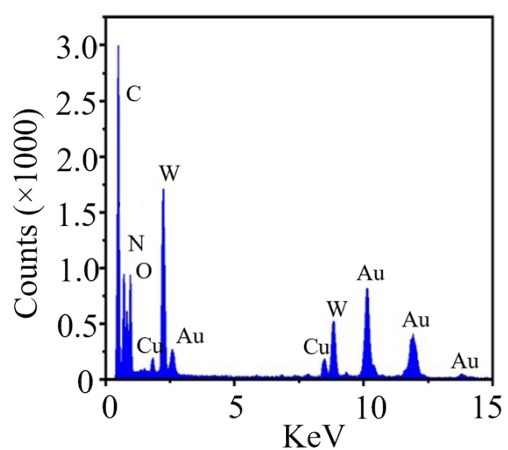


Fig. S4 EDX analysis of $\text{g-C}_3\text{N}_4/\text{WO}_3$ hybrid material and the peaks for Au and Cu result from the TEM analysis.

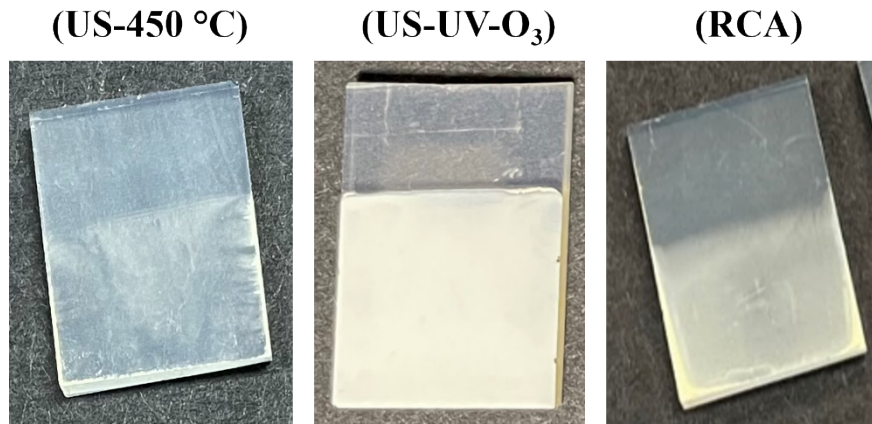


Fig. S5 Photographs of the g-C₃N₄/WO₃ film deposited using EPD onto FTO substrates, which was pre-treated using i) ultrasonic cleaning in DI water, and IPA (15 minutes each), followed by heating to 450 °C for 1 hour (US-450 °C), ii) ultrasonic cleaning in DI water, and IPA followed by 30 minutes UV-ozone treatment (US-UV-O₃), and iii) cleaning in a mixture of 20 mL NH₄OH (25%):10 mL H₂O: 5 mL H₂O₂ (30%) solution at 75 °C for 30 minutes (RCA).

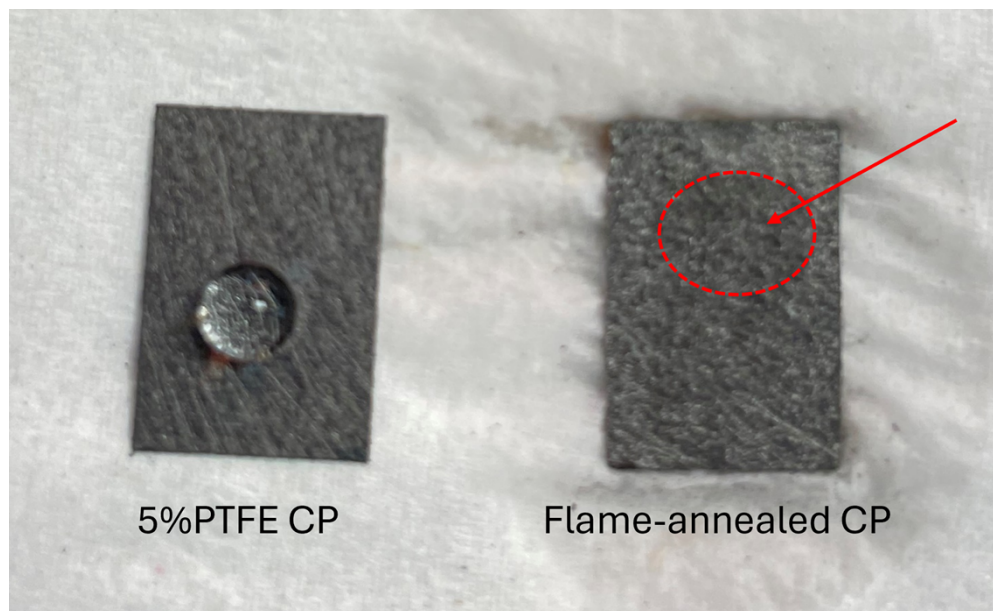


Fig. S6 Photograph shows a water droplet on 5%PTFE carbon paper and flame-treated carbon paper. The water droplet disperses completely and passes through the porous nature of the carbon paper, indicating a zero-contact angle. This suggests that the flame-annealed carbon paper has a high degree of hydrophilicity.

a



b

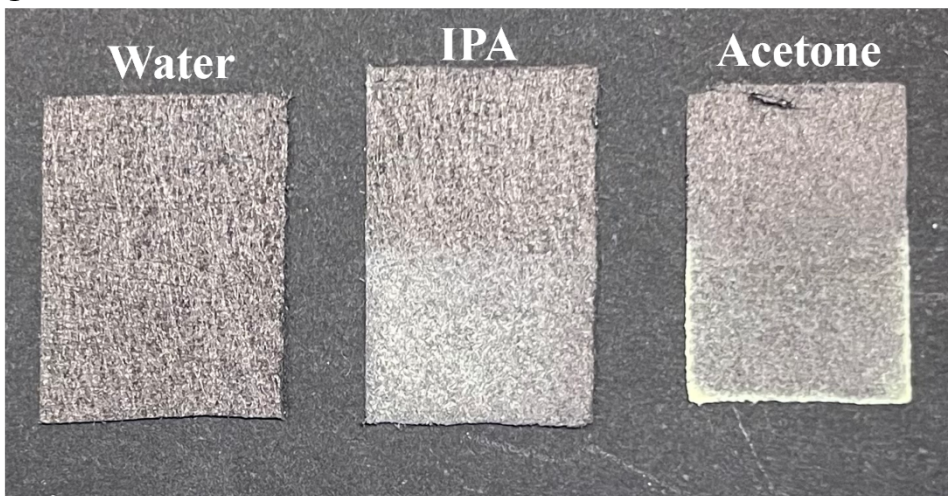


Fig. S7 a) Photographs of the C₃N₄/WO₃ suspension prepared in DI water, Isopropyl alcohol (IPA), and acetone, and b) Photographs of the EPD-coated thin film of C₃N₄/WO₃ on CP electrodes using the suspension prepared in (a) under 60 V for 1 minute.

a



b

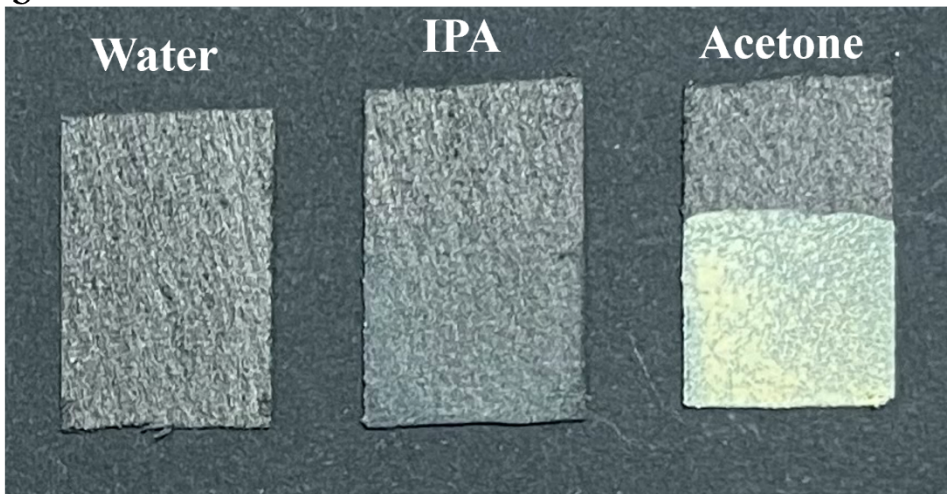


Fig. S8: a) Photographs of the C₃N₄/WO₃ suspension prepared in the presence of 10 mg I₂ in DI water, Isopropyl alcohol (IPA), and acetone, and b) Photographs of the EPD-coated thin film of C₃N₄/WO₃ on CP electrodes using the suspension prepared in (a) under 60 V for 1 minute.

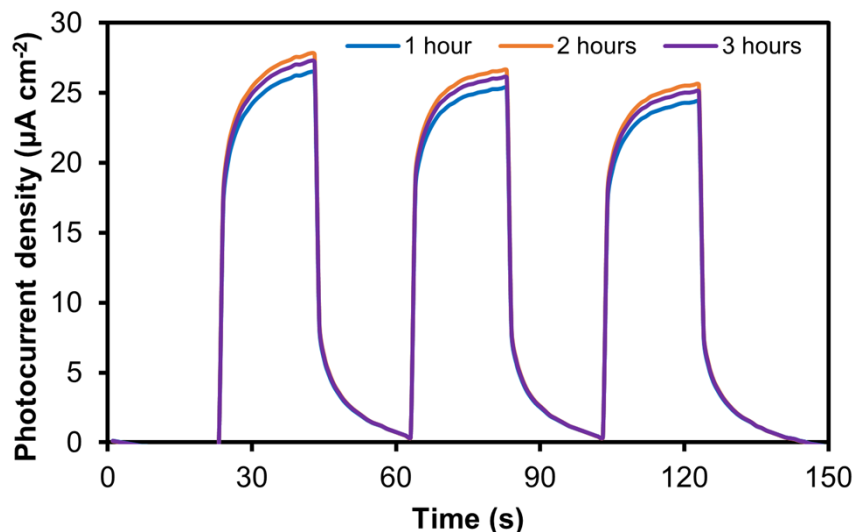


Fig. S9: Photocurrent responses of the $\text{g-C}_3\text{N}_4/\text{WO}_3$ thin film prepared from the suspension using various ultrasonication times from 1 hour to 3 hours, while adding I_2 at the end, followed by an additional minute of ultrasonication. All EPD coating was performed at 60 V for 1 minute.

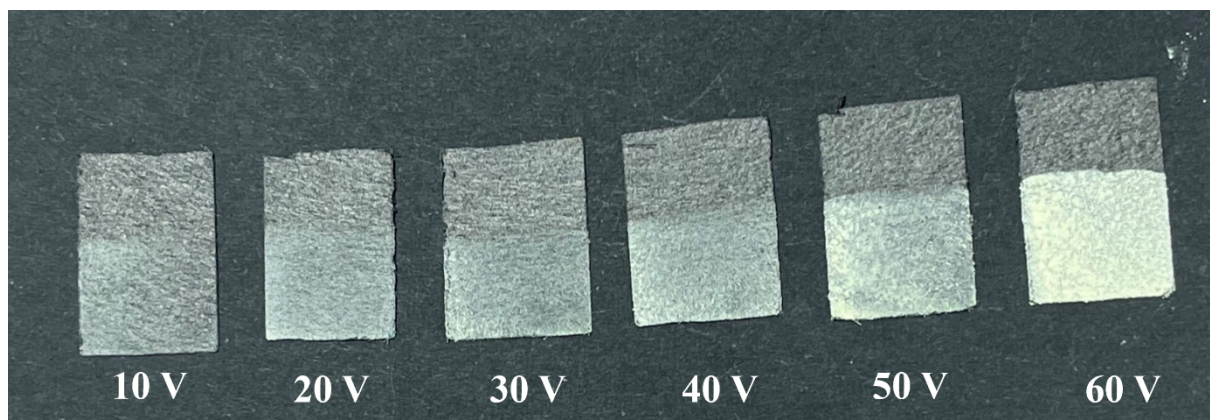


Fig. S10 Photograph of the $\text{C}_3\text{N}_4/\text{WO}_3$ thin films obtained by EPD coating under different voltages from 3 mg mL^{-1} suspension in acetone + I_2 at a constant deposition time of 1 minute.

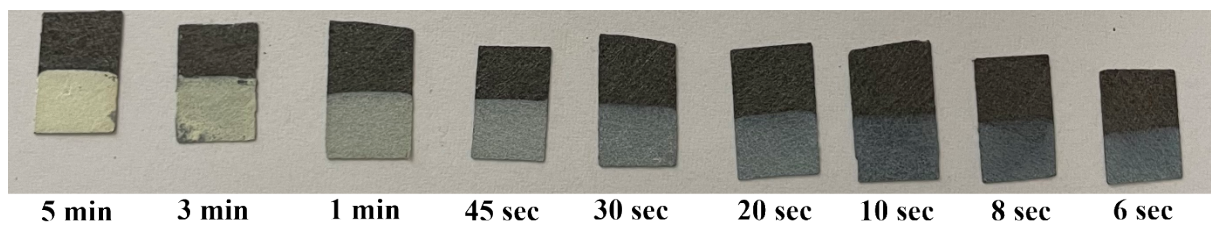


Fig. S11 Photograph of the C₃N₄/WO₃ thin film obtained by EPD coating under different deposition times ranging from 5 minutes to 6 seconds in 3 mg mL⁻¹ suspension in acetone + I₂ at a constant deposition voltage of 60 V.

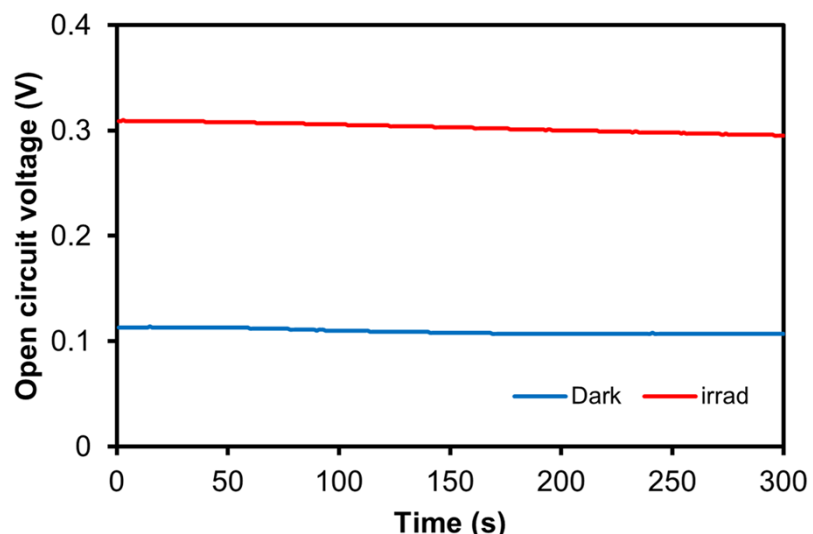


Fig. S12 Open circuit voltage of the g-C₃N₄/WO₃ hybrid photoanode under dark and irradiation conditions.

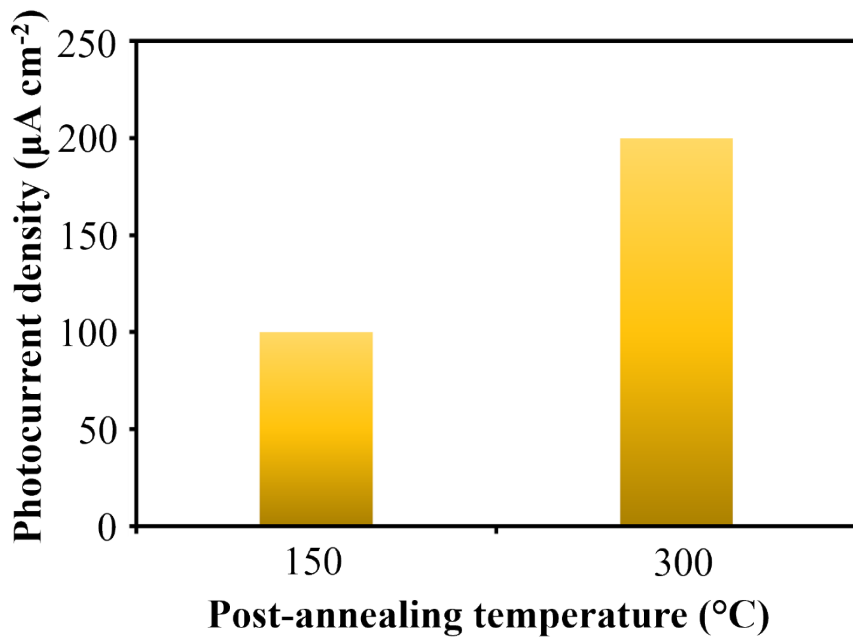


Fig. S13 Photocurrent responses of the g-C₃N₄/WO₃/CP photoanode post-annealed at 150 °C and 300 °C.

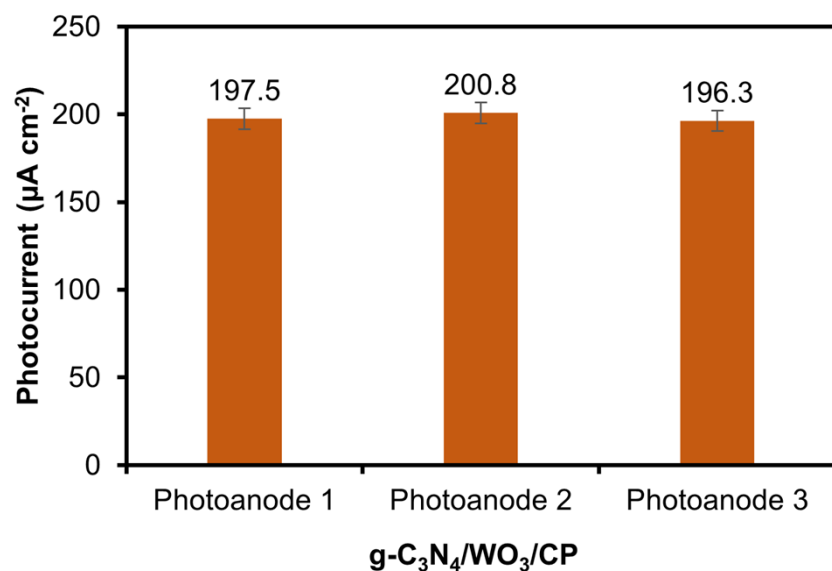


Fig. S14 Reproducibility test: Photocurrent responses of the three different g-C₃N₄/WO₃/CP photoanodes obtained in 0.1 M KOH solution containing 10% TEOA as a hole scavenger.

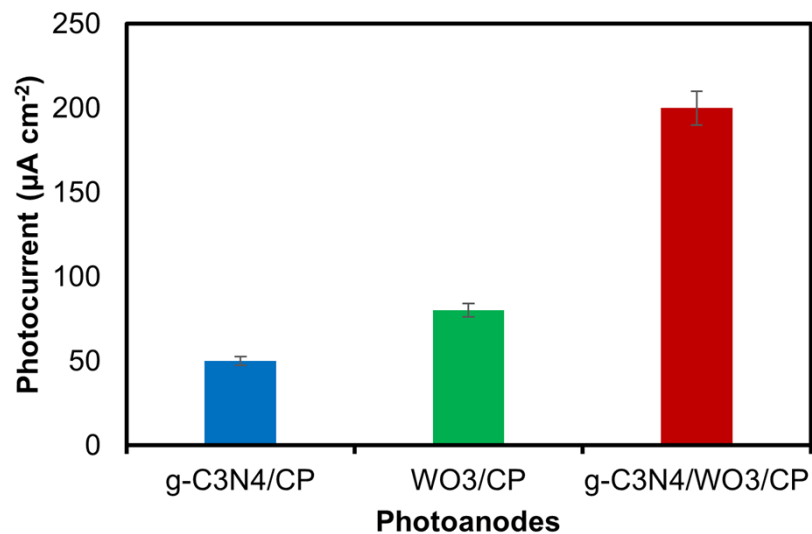


Fig. S15 Photocurrent responses of the g-C₃N₄/CP, WO₃/CP and g-C₃N₄/WO₃/CP electrodes.

Table S1. Experimental parameters used for the XPS measurements.

Region	Pass Energy (eV)	Dwell time (s)	Number of scans	Step energy (eV)
Survey	160	150	2	0.2
C 1s	20	60	20	0.1
O 1s	20	60	20	0.1
N 1s	20	60	20	0.1
W 4f	20	150	2	0.1

Table S2: Atomic percentage of surface composition from the g-C₃N₄ and g-C₃N₄/WO₃ junction samples.

Sample	C %	N %	O %	W %
g-C ₃ N ₄	49.5	49.9	0.6	-
g-C ₃ N ₄ /WO ₃	49.3	42.8	6.1	1.8

Peak model

The peak model for the carbon Nitride ($\text{g-C}_3\text{N}_4$) follows the previous work from David Morgan.³ A two-parameter Touggard ($U2$) background was used to determine fitting parameters for the satellite structure to the higher binding energy. The C 1 s spectra (Fig. 2a) were deconvoluted into six peaks ascribed to adventitious carbon (284.8 eV), C–OH, C–N–C and four satellite peaks. For the N 1s core level spectra, we use the three characteristic peaks for $\text{g-C}_3\text{N}_4$ ascribed to the sp^2 hybridized pyridine nitrogen in triazine rings (C=N–C), tertiary nitrogen N–(C)₃, and sp^3 terminal N (C–N–H), respectively. Also, the bulk material presents 4 satellite peaks observed at higher binding energies. A Lorentzian asymmetric (LA) Voigt type line shapes were used for the analysis of general form LA (α, β, m), where α and β define the spread of the tail on either side of the Lorentzian components and m is an integer between 0 and 499 specifying the width of the Gaussian used to convolute the Lorentzian peak (note the β parameter may be omitted). The fitting parameters used are as follows: LA(1.3, 243) for all peaks, including the satellite structure with the exception of C(1s) and N(1s) peaks at 288.1 and 398.7 eV, respectively, where LA(1.03,1.24,243) was used. Finally, a simple double separation was attributed to the W 4f spectra. We summarised the peak model and the fitting outcome in Tables S2 and S3.

Table S3: Peak model of C 1s spectra for the $\text{g-C}_3\text{N}_4$ and $\text{g-C}_3\text{N}_4/\text{WO}_3$ junction.

	Assignment	Positions Constraints	FWHM Constraints	Line shape
A	Adventitious C	284.8	1.4 ±0.2	LA(1.3, 243)
B	C-OH	A + 1.7 (± 0.2)	0.8 , 1.5	LA(1.3, 243)
C	C in C-N-C	A + 3.3 (± 0.2)	B * 1	LA(1.03,1.24,243)
D	Satellite	C + 5.1 (± 0.2)	2.0 , 2.7	LA(1.3, 243)
E	Satellite	D + 3.1	C*1	LA(1.3, 243)
F	Satellite	D + 5.7	C*1	LA(1.3, 243)
G	Satellite	D + 7.9	C*1	LA(1.3, 243)

Table S4: Peak model of N 1s spectra for the $\text{g-C}_3\text{N}_4$ and $\text{g-C}_3\text{N}_4/\text{WO}_3$ junction.

	Assignment	Positions Constraints	FWHM Constraints	Line shape
A	N in C–N–C	398.8 , 398.3	0.8 , 1.2	LA(1.03,1.24,243)
B	N in N-[C] ₃	A + 1.34 (± 0.2)	0.8 , 1.5	LA(1.3, 243)
C	N in C–N–H	A + 2.43 (± 0.2)	B * 1	LA(1.3, 243)
D	Satellite	418.9 , 391.8 (± 0.2)	2.0 , 2.7	LA(1.3, 243)
E	Satellite	D + 3.1	C*1	LA(1.3, 243)
F	Satellite	D + 5.7	C*1	LA(1.3, 243)
G	Satellite	D + 7.9	C*1	LA(1.3, 243)

Table S5: Peak position, FWHM and percentage of different components from the W 4f 1s for WO_3 and g-C₃N₄/WO₃ junction.

Component		WO ₃	g-CN/WO ₃
W 4f 7/2	Position (eV)	36.0	35.8
	FWHM (eV)	1.3	0.9
	Area (%)	55.2	54.4
W 4f 5/2	Position (eV)	37.9	37.8
	FWHM (eV)	1.3	0.9
	Area (%)	41.4	41.7
W 3p	Position (eV)	41.6	41.5
	FWHM (eV)	1.8	1.7
	Area (%)	3.4	3.9

Table S6: Peak position, FWHM and percentage of components from the O 1s for WO_3 and g-C₃N₄/WO₃ junction.

Component		WO ₃	g-C ₃ N ₄ /WO ₃
W-O-Lattice	Position (eV)	530.8	530.6
	FWHM (eV)	1.2	1.4
	Area (%)	80	57.7
W-O (H ₂ O)	Position (eV)	531.8	531.5
	FWHM (eV)	2.0	1.9
	Area (%)	20.0	35.1
g-CN-O	Position (eV)	-	533.1
	FWHM (eV)	-	1.5
	Area (%)	-	7.2

Table S7: Peak position, FWHM and percentage of different components from the C 1s for the g-C₃N₄ and g-C₃N₄/WO₃ heterojunction.

Component		g-C ₃ N ₄	g-CN/WO ₃
Adventitious C	Position (eV)	284.8	284.8
	FWHM (eV)	1.08	1.36
	Area (%)	5.0	40.7
C-OH	Position (eV)	286.5	286.3
	FWHM (eV)	1.5	1.28
	Area (%)	1.9	1.7
C in C-N-C	Position (eV)	288.1	288.3
	FWHM (eV)	0.97	1.16
	Area (%)	81.2	53.3
Satellite	Position (eV)	293.1	293.5
	FWHM (eV)	1.74	1.31
	Area (%)	3.9	1.6
Satellite	Position (eV)	294.3	294.66
	FWHM (eV)	1.74	1.32
	Area (%)	3.3	1.1
Satellite	Position (eV)	296.10	296.10
	FWHM (eV)	1.74	1.36
	Area (%)	1.4	0.3
Satellite	Position (eV)	299.4	299.4
	FWHM (eV)	2.75	2.15
	Area (%)	3.2	1.2

Table S8: Peak position, FWHM and percentage of different components from the N 1s for the g-C₃N₄ and g-C₃N₄/WO₃ junction.

Component		g-C ₃ N ₄	g-C ₃ N ₄ /WO ₃
N in C–N–C	Position (eV)	398.6	398.8
	FWHM (eV)	1.08	1.25
	Area (%)	63.6	65.0
N in N-[C] ₃	Position (eV)	399.93	400.1
	FWHM (eV)	1.30	1.35
	Area (%)	10.8	13.40
N in C–N–H	Position (eV)	401.03	401.2
	FWHM (eV)	1.30	1.35
	Area (%)	11.1	10.70
Satellite	Position (eV)	404.24	404.5
	FWHM (eV)	2.6	2.69
	Area (%)	9.1	7.1
Satellite	Position (eV)	407.34	407.55
	FWHM (eV)	2.7	2.7
	Area (%)	3.3	2.2
Satellite	Position (eV)	409.94	410.15
	FWHM (eV)	2.3	2.3
	Area (%)	0.7	0.2
Satellite	Position (eV)	412.14	412.35
	FWHM (eV)	2.4	2.7
	Area (%)	1.6	1.4

Table S9: EPD-coated film of C₃N₄/WO₃ on CP under various deposition times at a constant electric potential of 60 V and their corresponding weight loading averaged from the triplicate samples. The photocurrent density was also obtained from three samples of each deposition time and reported as the average.

EPD deposition time (seconds)	Amount of C ₃ N ₄ /WO ₃ material deposited (mg cm ⁻²)			Average (mg cm ⁻²)	Photocurrent density (μA cm ⁻²)
	S1	S2	S3		
6	0.04	0.050	0.040	0.043	145.50
8	0.07	0.078	0.073	0.073	171.60
10	0.104	0.100	0.105	0.103	200.00
20	0.23	0.21	0.190	0.210	132.00
30	0.37	0.35	0.290	0.336	118.80
45	0.62	0.58	0.56	0.586	40.90
60	0.98	0.90	0.93	0.930	35.60
180	2.45	2.31	2.37	2.376	18.50
300	4.38	4.03	4.20	4.203	14.50

Statistical analysis:

A one-way ANOVA was performed for each independent variable to assess its impact on the dependent variable of photocurrent density. The analysis included F-values, F-critical values, P-values, and effect size (η^2). Statistical significance was determined based on a predefined significance threshold (typically $\alpha = 0.05$).

Table S10: The results of the ANOVA tests are summarized below:

Independent variable	F-value	F-crit value	P-value	effect size (η^2)	Significant (yes/no)
Substrate pre-treatment	812.07	5.14	4.98E-08	0.996	yes
Suspension solvent	11075.70	5.14	1.98E-11	0.999	yes
Suspension concentration	7736.80	3.1	1.30E-20	0.998	yes
Deposition time	18259.69	2.5	1.43E-33	0.999	yes
Post-annealing temperature	17262.95	7.7	2.01E-08	0.997	yes

Table S11: Comparison of the PEC activities of present g-C₃N₄ and g-C₃N₄/WO₃ photoanodes with earlier reports fabricated photoelectrodes using EPD.

Photoanode	Suspension medium	Applied voltage (V)	Deposition time	Photocurrent density ($\mu\text{A cm}^{-2}$)	Ref.
g-C ₃ N ₄ /Al plate	Water	2	24 hours	-	⁴
m-C ₃ N ₄ /SST wire	Water	20	1 hour	-	⁵
g-C ₃ N ₄ /SnO ₂ /FTO	IPA + Mg(NO ₃) ₂	30	5 minutes	150	⁶
g-C ₃ N ₄ /FTO	Toluene	200	60 minutes	65	⁷
g-C ₃ N ₄ /ITO	Acetone + I ₂	25	10 seconds	25	⁸
g-C ₃ N ₄ /C dots/PET/ITO	Acetone + I ₂	10	10 minutes	38	⁹
Ni ₃ S ₂ /g-C ₃ N ₄ /FTO	Acetone + I ₂	20	5 minutes	18	¹⁰
g-C ₃ N ₄ /CP	Acetone + I ₂	60	10 seconds	50	This work
WO ₃ /CP	Acetone + I ₂	60	10 seconds	80	This work
g-C ₃ N ₄ /WO ₃ /CP	Acetone + I ₂	60	10 seconds	200	This work

Table S12: The photoanode current density comparison of the present EPD method with the earlier reports prepared photoanode using various methods.

Deposition method	Photoanodes	Photocurrent density ($\mu\text{A cm}^{-2}$)	Ref.
Thermal vapour condensation	g-C ₃ N ₄ /FTO	50	¹¹
Thermal vapour condensation	g-C ₃ N ₄ /FTO	120	¹²
Microcontact-printing	g-C ₃ N ₄ /FTO	30.2	¹³
Direct growth	g-C ₃ N ₄ /FTO	22	¹⁴
Solvothermal method	g-C ₃ N ₄ /FTO	3.6	¹⁵
Electrospinning	CPVP/g-C ₃ N ₄ /ITO	6.6	¹⁶
Liquid-based growth	S-g-C ₃ N ₄ /FTO	100	¹⁷
Doctor-blade	g-C ₃ N ₄ /FTO	3	¹⁸
Seed growth	g-C ₃ N ₄ /FTO	116	¹⁹
EPD	g-C ₃ N ₄ /WO ₃ /CP	200	This work

References:

- 1 T. M. LeMercier, M. Thangamuthu, E. C. Kohlrausch, Y. Chen, C. T. Stoppiello, M. W. Fay, G. A. Rance, G. N. Aliev, W. Theis, J. Biskupek, U. Kaiser, A. E. Lanterna, J. A. Fernandes and A. N. Khlobystov, *Sustain Energy Fuels*, 2024, **8**, 1691–1703.
- 2 M. Thangamuthu, K. Vankayala, L. Xiong, S. Conroy, X. Zhang and J. Tang, *ACS Catal*, 2023, **13**, 9113–9124.
- 3 D. J. Morgan, *Surface Science Spectra*, 2021, **28**, 014007.
- 4 M. Ghaemmaghami, Y. Yamini, H. Amanzadeh and B. Hosseini Monjezi, *Chemical Communications*, 2018, **54**, 507–510.
- 5 D. B. Hernández-Uresti, A. Vázquez, S. Obregón and M. A. Ruíz-Gómez, *Mater Lett*, 2017, **200**, 59–62.
- 6 Y. J. Seo, P. K. Das, M. Arunachalam, K.-S. Ahn, J.-S. Ha and S. H. Kang, *Int J Hydrogen Energy*, 2020, **45**, 22567–22575.
- 7 J. Xu and M. Shalom, *ACS Appl Mater Interfaces*, 2016, **8**, 13058–13063.
- 8 P. Wongchaiya, T. K. N. Nguyen, P. Sujaridworakun, S. Larpkiattaworn, T. S. Suzuki and T. Uchikoshi, *Advanced Powder Technology*, 2024, **35**, 104460.
- 9 Y. Wei, Z. Wang, J. Su and L. Guo, *ChemElectroChem*, 2018, **5**, 2734–2737.
- 10 M. Zhao, X. Yang, X. Li, Z. Tang and Z. Song, *Journal of Electroanalytical Chemistry*, 2021, **893**, 115324.
- 11 J. Bian, L. Xi, J. Li, Z. Xiong, C. Huang, K. M. Lange, J. Tang, M. Shalom and R.-Q. Zhang, *Chem Asian J*, 2017, **12**, 1005–1012.
- 12 J. Bian, Q. Li, C. Huang, J. Li, Y. Guo, M. Zaw and R.-Q. Zhang, *Nano Energy*, 2015, **15**, 353–361.
- 13 J. Liu, H. Wang, Z. P. Chen, H. Moehwald, S. Fiechter, R. van de Krol, L. Wen, L. Jiang and M. Antonietti, *Advanced Materials*, 2015, **27**, 712–718.
- 14 L. Ye and S. Chen, *Appl Surf Sci*, 2016, **389**, 1076–1083.
- 15 X. Xie, X. Fan, X. Huang, T. Wang and J. He, *RSC Adv*, 2016, **6**, 9916–9922.
- 16 Y. Wang, X. Zhao, Y. Tian, Y. Wang, A. K. Jan and Y. Chen, *Chemistry – A European Journal*, 2017, **23**, 419–426.
- 17 Y. Fang, X. Li and X. Wang, *ACS Catal*, 2018, **8**, 8774–8780.
- 18 G. Peng, L. Xing, J. Barrio, M. Volokh and M. Shalom, *Angewandte Chemie International Edition*, 2018, **57**, 1186–1192.
- 19 G. Peng, J. Albero, H. Garcia and M. Shalom, *Angewandte Chemie International Edition*, 2018, **57**, 15807–15811.